Lab on a Chip

PAPER

View Article Online
View Journal | View Issue

Cite this: *Lab Chip*, 2016, **16**, 4406

Integrative optofluidic microcavity with tubular channels and coupled waveguides *via* two-photon polymerization†

Yonglei Li,[ab] Yangfu Fang,[a] Jiao Wang,[ac] Lu Wang,[a] Shiwei Tang,[a] Chunping Jiang,[b] Lirong Zheng[c] and Yongfeng Mei*[a]

Received 14th September 2016,
Accepted 10th October 2016

DOI: 10.1039/c6lc01148a

www.rsc.org/loc

Miniaturization of functional devices and systems demands new design and fabrication approaches for lab-on-a-chip application and optical integrative systems. By using a direct laser writing (DLW) technique based on two-photon polymerization (TPP), a highly integrative optofluidic refractometer is fabricated and demonstrated based on tubular optical microcavities coupled with waveguides. Such tubular devices can support high quality factor (*Q*-factor) up to 3600 *via* fiber taper coupling. Microtubes with various diameters and wall thicknesses are constructed with optimized writing direction and conditions. Under a liquid-in-tube sensing configuration, a maximal sensitivity of 390 nm per refractive index unit (RIU) is achieved with subwavelength wall thickness (0.5 μm), which offers a detection limit of the devices in the order of 10^{-5} RIU. Such tubular microcavities with coupled waveguides underneath present excellent optofluidic sensing performance, which proves that TPP technology can integrate more functions or devices on a chip in one-step formation.

Introduction

Optical sensing, by virtue of its immunity to electromagnetic interference and multiplexed detection,[1] has attracted considerable attention in both fundamental research and practical applications.[1–6] Interesting optical structures, like surface plasmons,[4,7,8] interferometers,[9,10] optical waveguides[11] and resonators,[12–14] have been intensively investigated to realize sensing capability. Therein, with the advantages of small physical sizes and superior performance, optical resonator devices can be utilized to sensitively perceive the surrounding changes, including physical, chemical or biological properties, and can be further miniaturized and integrated as lab-on-a-chip devices.[15–18]

Environmental sensing based on optical resonators originates from the interaction between surrounding media and the resonator's evanescent light field, which behaves as the changes (*e.g.* shift or broadening) of its resonance modes.[13,19–21] In a whispering gallery mode (WGM) resonator, light propagates and accumulates along the cavity surface by total internal reflection.[20] The evanescent part would leak out and penetrate into the surrounding environment, which thus influences the WGM and induces spectral shifts.[19,21–26] WGM resonators like microspheres,[22,27] disks[28] and toroids[13,20] have presented high sensitivities as well as tubular microcavities, which are expected to be pronounced with a stronger evanescent field in tubular microcavities.[21,26] The relatively thin wall thickness (sub-microns) of a microtube can enable more energy to leak out for the interaction with surrounding media. In another way, tubular microcavities with their unique hollow structures[19,21,29,30] can inherently act as optofluidic channels to integrate both optic and fluidic functions.[21,29,30] Currently, tubular microcavities are mainly fabricated by the capillary pulling method[1,14,16,23] and rolled-up nanotechnology.[12,17,29,31] Microcapillary cavities present advantages such as an easy process and higher sensing performance,[23] while rolled-up tubular cavities benefit from the capability of on-chip integration.[17] Actually, with the development of micromachining and microelectronics, there emerges a novel method, direct laser writing (DLW), for tubular microcavity fabrication. DLW is a manufacture technology for three-dimensional (3D) micro and nanostructures based on the two-photon polymerization (TPP) principle, which has been applied to the fabrication of various 3D microstructures,[32–36] such as photonic crystals,[34] metamaterials,[35] waveguides,[36] microdisks,[18,37–40] microtoroids,[41] *etc.* For microtube fabrication, TPP possesses unique advantages. Compared with capillary pulling, TPP is compatible

[a] *Department of Materials Science & State Key Laboratory of ASIC and Systems, Fudan University, Shanghai 200433, China. E-mail: yfm@fudan.edu.cn*
[b] *Key Laboratory of Nanodevices and Applications, Suzhou Institute of Nano-tech and Nano-bionics, Chinese Academy of Sciences, Suzhou 215125, China*
[c] *School of Information Science & Technology, Fudan University, Shanghai 200433, China*

† Electronic supplementary information (ESI) available. See DOI: 10.1039/c6lc01148a

with microelectronic processes and is ready for on-chip integration. Meanwhile, though rolled-up technology can realize the optimal sensing liquid-in-tube configuration, plenty of complex, time-consuming additional work has to be done, such as supporting socket fabrication, microtube transfer by micro-manipulation, microtube re-fixing by photolithography and oxide deposition.[17] Compared with this technology, TPP is an easy and flexible fabrication process with high accuracy, and can easily replace and omit many tedious and error-prone sequential steps like multiple planar lithography and etching. This can also improve the fabrication progress and success rate.

Here, the TPP method is employed to construct tubular optical microcavities integrated with coupled waveguides, liquid reservoirs and fluidic channels. Such tubular cavities are optimized in terms of their uniformity and reliability using two writing routes and can support the highest quality factor (Q) values up to 3600. By monitoring WGM position shifts on the liquid-in-tube configuration, a maximum sensitivity of 390 nm per refractive index unit (nm per RIU) is achieved in the fabricated 0.5 μm-thick-walled tubular microcavities (diameter = 20 μm). Finally, a fully integrated tubular microcavity sensor is realized and directly written together with a waveguide underneath by utilizing TPP. Experimental results agree well with the corresponding theoretical simulations based on the Mie scattering theory. Our results reveal that the monolithic tubular microcavity sensors fabricated by TPP could be one of the perfect candidates for on-chip optofluidic applications, while the TPP method can be an effective approach for design and manufacture of multifunctional optical devices on the micro and nanoscale.

Experimental section

Fabrication of designed devices

The designed tubular device is predominantly composed of a tubular microcavity and an affiliated fluidic reservoir. As sketched in Fig. 1(a), a designed hollow tube acts as the optical microcavity and fluidic channel, while the supporting pedestals are located on both sides to avoid resonant WGMs leaking into substrates. Besides, the reservoirs are introduced for better liquid injection and guidance of injected liquids flowing into the tube, which can enable the sensing test under the liquid-in-tube configuration. The reservoir is hemispherical so that liquids could easily flow into the tube. All components mentioned above are monolithically constructed on a common fused glass substrate.

The Photonic Professional GT DLW system (Nanoscribe Company) employed here is equipped with a pulsed erbium-doped femto fiber laser (centred at 780 nm with a repetition rate of 80 MHz and 100 femtoseconds pulse duration) as the exposure source, which can polymerize the applied negative photoresist (Nanoscribe IP-L 780) through a two-photon absorption-induced polymerization process. The refractive index n of the resist after polymerization is about 1.48. An oil-immersion lens (Leica, 100×, numerical aperture NA = 1.4) is

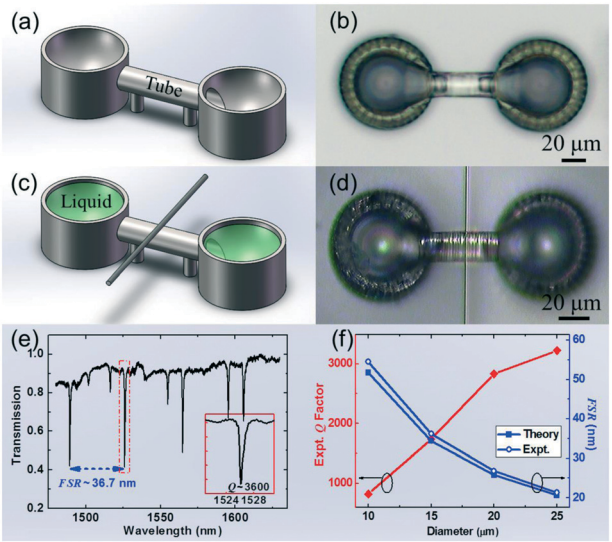

Fig. 1 Design and characterization of TPP devices. (a) Schematic diagram and (b) optical microscopy image of a tubular microcavity with liquid reservoirs. The tube has a diameter (D) of 20 μm and a wall thickness (T) of 0.5 μm. (c) Sketch and (d) optical microscopy image of the designed device coupled with a vertically placed fiber taper under a liquid-in-tube configuration for transmission spectral measurement. (e) A representative transmission spectrum of a fabricated tubular microcavity with D = 14 μm and T = 0.6 μm. The inset shows one individual WGM peak centered at 1526 nm for Q-factor calculation. (f) Q-factor (red line) and FSR (blue line) of tubular microcavities with a fixed wall thickness of 0.5 μm as a function of tube diameter.

used to tightly focus the laser into the photoresist. The resist at the focal spot of the laser can be polymerized during exposure and further retained in the subsequent development process. The target structure can be fabricated by scanning the laser beam throughout the resist guided by NanoWrite software with the 3D structure designed by Describe 2.1 software.

Device fabrication began from the cleaning of a fused glass substrate (n = ~1.5) with acetone and isopropanol (IPA). After drying, the substrate was dripped with a drop of IP-L 780 resist in its center and fixed to the sample holder of the DLW system. The writing process was performed according to the designed structure (Fig. 1(a)) with about 6 milli-watt average laser power and 200 μm s^{-1} scanning velocity. After writing, the resist was developed by immersing in a propylene glycol methyl ether acetate (PGMEA) solution for 30 minutes, followed by rinsing in a bath of IPA for 15 minutes. An optical microscopy image of such a fabricated device is displayed in Fig. 1(b). Considering the ellipsoid-shaped focal spot of the exposure laser (voxels are necessarily taller than they are wider), some modifications have been made toward the pre-designed microtube part to ensure the roundness of the fabricated microtube (in other words, to ensure that the cross-section of the tubular part has the same and constant thickness). The typical hydrophobicity of this microsystem is attributed to the intrinsic properties of the photoresist. A fiber taper is vertically placed on top of the structure, and adopted to measure the transmission spectra

as shown in Fig. 1(c), while the corresponding optical microscopy image is presented in Fig. 1(d), where a fiber taper is closely placed on the top of the tube as expected.

Optical measurement setup

In order to characterize the WGM properties and sensing capability of the fabricated devices, transmission spectral measurements at near infrared wavelengths (from 1480 nm to 1620 nm) are performed through the evanescent field coupling method.[20] As shown in Fig. S1,† a single-mode, tunable external-cavity laser (Ando 4321D, linewidth 200 kHz) was utilized to evanescently excite the WGM coupling of the microtube cavity with a tapered optical fiber. The fiber taper, with a waist diameter of approximately 1 μm, was home-prepared by heating and stretching a section of a commercial single-mode fiber (Corning SMF-28e). Some of the light in the fiber escaped from the waist, interacted with and entered into the orthogonal microtube *via* coupling (Fig. 1(d)). Then, the residual light in the fiber was converted into electrical signals *via* a low-noise indium gallium arsenide photoelectric detector (Thorlabs PDA10CS-EC), displayed in a digital multimeter (Agilent 34401A), collected and real-time monitored by a computer through LabVIEW and a GPIB (General-Purpose Interface Bus) data acquisition card (National Instruments). By continuously sweeping the wavelengths of the laser over a long spectral range, light at certain wavelengths could couple into the tubular microcavity resonator and discrete WGMs can be observed as Lorentzian-shaped dips in the transmission spectrum as shown in Fig. 1(e). In order to avoid any distortions of the line shapes caused by resonant built-up thermal effects within the resonators, low output laser power was adopted here.[42]

Optofluidic setup

Taking advantage of tubular microcavities for optofluidic application,[21] a fluidic sensing test was demonstrated under a liquid-in-tube configuration (Fig. 1(c)), which was accomplished by injecting liquids into one reservoir using a stretched glass capillary with the help of a microsyringe. The capillary was mounted on a piezoelectric positioning stage and moved close to the resonator so that the small end could reach the reservoir (see Fig. S2(a)†), while the other end was connected to the syringe pump. By means of injection force and capillary force between the capillary end and the reservoir, liquid could be slowly injected into the reservoir, and then fill the whole microtube (see Fig. S2(b)† without liquid and S2(c)† with IPA liquid). Subsequently, liquid could be drained from the reservoir in the same way. The fabricated structures present excellent mechanical stabilities without any distortion or collapse under repeated liquid injections, extractions and measurements. Besides, the sizes of the solid tubular parts have no obvious changes during the entire processes, so the slight interaction between liquids and the structures, with the corresponding influences, will not be considered here. Various typical liquids with different refractive indices[29] (de-ionized (DI) water/IPA mixture (1 : 8 in volume) with n = 1.370, pure IPA with n = 1.375 and glycol/IPA mixture (2 : 9 in volume) with n = 1.385) were adopted as test agents to verify the sensitivities in our experiments. Though the microcavity is tested hydrophobic to water, water-based solution sensing can also be realized after a simple surface modification process.[19,43,44] For example, a thin layer coating of metal oxides (like several nanometers Al_2O_3 or TiO_2) by atomic layer deposition can dramatically enhance the inner surface hydrophilic ability and water wettability.[43,44] In addition, this mild modification process has little influence on the size and performance of the tubular microcavity.

Results and discussion

Characterization of transmission spectrum

With the above testing method, a representative transmission spectrum of our fabricated device reveals the resonant WGMs as shown in Fig. 1(e). The diameter D of the tubular microcavity is designed as 14 μm and measured as 13.7 μm, while the wall thickness T is 0.6 μm. The experimental free spectral range ($\Delta\lambda_{FSR}$ = 36.7 nm) agrees with the simulation results ($\Delta\lambda_{FSR}$ = 36.5 nm) using the theoretical formula $\Delta\lambda_{FSR} = \lambda^2/(\pi nD)$,[29,45–48] where λ is the resonance wavelength. The small difference may result from the tiny size error between the pre-designed and final fabricated structures. The inset of Fig. 1(e) discloses an individual WGM peak centered at 1526 nm with the full width at half maximum (FWHM) $\Delta\lambda$ = ~0.42 nm, which corresponds to a Q-factor of 3600 according to $Q = \lambda/\Delta\lambda$. Taking unavoidable coupling loss induced by the tapered fiber into consideration ($1/Q_m = 1/Q_{in} + 1/Q_c$),[45,46,49] where Q_m is the experimentally measured Q value, Q_{in} is the intrinsic Q value of the resonator, and Q_c is the Q value induced by coupling, under critical-coupling conditions,[45] $Q_{in} = Q_c$, $Q_m = Q_{in}/2$, and under over-coupling contact conditions, $Q_{in} > Q_c$, $Q_m < Q_{in}/2$; thus, the intrinsic value Q_{in} of the fabricated microtube can reach up to 7200.

Fig. 1(f) presents the measured Qs and FSRs of tubular microcavities with a wall thickness of 0.5 μm and various diameters (D = 10, 15, 20 and 25 μm, the representative tube wall picture is shown in Fig. S3†). There exist many factors affecting the Q-factors in a microcavity, such as radiation loss, material absorption and others. Taking the relatively high theoretical material-limiting Q (about 10^5–10^7) of referenced polymer microcavities[37,39] and the transparency of IP-L 780 in the 1500–1600 nm band into consideration, material absorption cannot be preliminarily regarded as the main loss mechanism. Also, B. E. Little has stated that when D is small enough (usually $D < 25$ μm), the main factor influencing and limiting Q is the radiation loss by total internal reflection, and it decreases gradually accompanied by the increase of diameter D.[46] Here, the experimental increasing trend (rhombus and red line) of the Q-factors along with the diameter increase agrees well with this radiation-loss-limiting theory and tendency. Meanwhile, the change of FSRs is

inversely proportional to D according to $\Delta\lambda_{FSR} = \lambda^2/(\pi nD)$. It is found that the measured FSRs (empty circle and blue line) of the tubular microcavities with various diameters agree well with the corresponding calculated values (solid square and blue line). The slight differences between experiments and calculation may result from the small diameter variation of the fabricated structures, which seems more obvious when D is smaller.

Tube quality *vs.* writing direction

To achieve the best quality of our structure, the writing route under a continuous mode was adopted in our experiments. However, in a 3D tubular structure, there are still two directions to continuously write tube walls as shown in Fig. 2(a) and (b), which are along the circumference (AC) and along the axial direction (AD), respectively. The former writing method is along the circumference of the transverse section of the microtube while the latter is along the axis of the microtube. Due to the mechanical movements and exposure deviations during the DLW process, writing traces can inevitably be recorded on the fabricated devices' surfaces. Fig. 2(c) and (d) present scanning electron microscopy (SEM) images of the fabricated tube wall surfaces with the diameter of 20 μm and tube wall thickness of 0.5 μm by the above two methods. Writing traces can be observed on the surfaces of both tubes, whose enlarged views are shown at the top-right insets. The surface roughness caused by the regular lines along the writing direction is about several hundred nanometers, and it will certainly influence the optical resonance properties of the fabricated microtubes. The traces or lines caused by the AC writing method are parallel to the light propagation direction and thus have little influence on the resonance performance of the microtubes. The situation for the AD writing method is distinct because the traces or lines are perpendicular to the light propagation direction in the fabricated tubular structures, which could heavily scatter the circulating light and reduce the resonance quality. Resonant WGMs of the microtubes fabricated by the AC method are shown in Fig. 2(e). However, there are no WGMs detected in the microtubes fabricated by the AD writing method as shown in Fig. 2(f). In order to prove the reliability, three typical data points were measured (marked by red, blue and yellow spots) and there is almost no difference in their resonance properties. Thus, it is proven that the AC writing method is a feasible way for fabricating tubular microcavities with obvious resonant WGMs. In addition, the surface roughness (traces or lines) caused by both writing methods can also be reduced through an additional subsequent proper annealing reflow treatment, which can further improve the resonance performance.

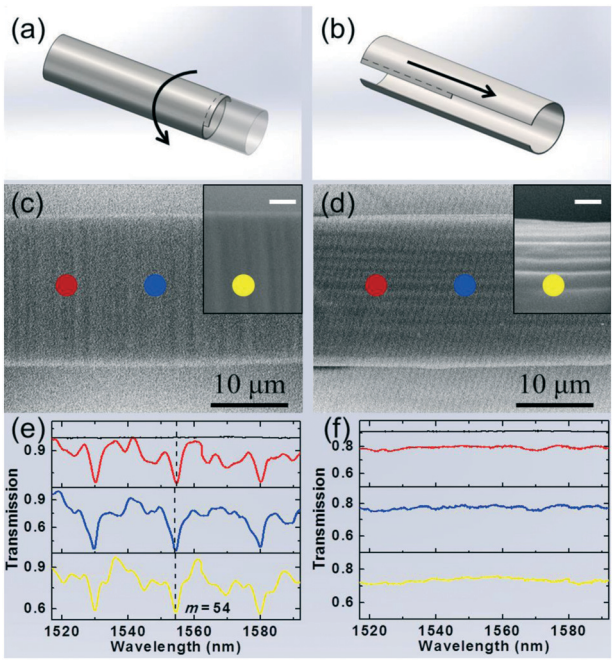

Fig. 2 Writing directions on a tube. Two writing directions are adopted to fabricate tubes: (a) along the circumference (AC) and (b) along the axial direction (AD). SEM images of the fabricated tubular wall surfaces along the writing directions of (c) AC and (d) AD. Their insets show the enlarged surface topography (scale bar is 2 μm). Transmission spectra (e and f) measured in different positions marked in (c) and (d), respectively. The black curves represent the transmission spectra of a standalone tapered fiber for reference. The colored lines in (e) and (f) correspond to the points in (c) and (d) with the same color.

In order to exclude the influence of holders (inset in Fig. 3(a)) on transmission spectra, further investigation on the uniformity and reliability of the fabricated tubular structures was conducted by using mapping of transmission spectra along with the tube axis. Normally in a tubular microcavity, TM modes (transverse magnetic modes, whose electric field vectors are defined parallel to the microtube axis here) have higher intensity confined in the microtube itself compared with TE modes (transverse electric modes, whose magnetic field vectors are parallel to the tube axis) and, due to the non-continuous electric field of TE modes at the wall–air interface which will cause higher loss, TM modes possess higher Q-factors than TE modes.[19,21] Considering the thin-walled tubular microcavities with relatively low Q-factors, TM modes are usually adopted in real experiments to characterize microtube performance, because they are much more easily observed first and detected than TE modes.[15,19,21,25,29,48] Fig. 3(a) presents the TM mode position (solid circle and black line) with the azimuthal number m = 54 in a tubular microcavity with the diameter of 20 μm and wall thickness of 0.5 μm. The mode number m is derived from the formulas $\Delta\lambda_{FSR} = \lambda^2/(\pi nD)$ and $m\lambda = \pi nD$.[21,48] Based on the equation $m\lambda = \pi nD$, it can also be deduced with the diameter variation (solid square and blue line) of the fabricated tubes between two holders. It is noted that there is a smaller variation of tube diameter in the center part (gray area) compared with the part close to the holders. The maximum deviation value for m = 54 mode position (average position: 1554.3 nm) is about 7.0 nm, which corresponds to a diameter variation of 92 nm. In the central part (gray area), the diameter variation

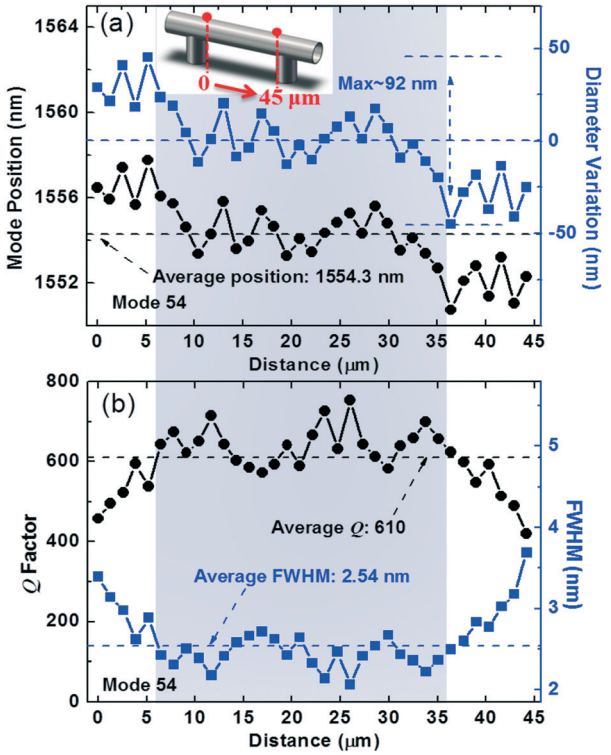

Fig. 3 Optical characterization of a tubular microcavity. (a) Mode position (black) and the corresponding deduced diameter variation (blue) for the resonance mode m = 54 along with a tubular microcavity axis (D = 20 μm, T = 0.5 μm, length = 45 μm). Inset shows the practical structure and the distribution of test positions. (b) The corresponding Q-factors (black) and FWHMs (blue) for the tube tested above. The central gray area in both figures indicates favorable repeatability and reliability.

is 40.8 nm, which is much smaller. Such difference may result from different mechanical deformations in the development and drying fabrication processes. Meanwhile, the corresponding Q-factors (solid circle and black line) along with FWHMs (solid square and blue line) are shown in Fig. 3(b). In the central part, there is a very small fluctuation of Q-factors near the average value, which indicates the favorable repeatability and reliability of our fabricated structure. Once close to the holders, Q-factors shift a lot as well as the FWHM values. The former decrease and the latter increase. The central part is almost 30 μm long, which can guarantee our device measurement for fluidic application.

Liquid sensing capability

The sensing performance and mechanism have been investigated with various configurations based on rolled-up microtubes in previous studies.[17,21] The liquid-in-tube configuration of tubular microcavities as one of the optofluidic refractometers resulted in excellent figures of merit of sensitivity and Q-factors. In order to probe such sensing capability of our fabricated tubes, WGM shifts were monitored by measuring transmission spectra with different liquid media. A large refractive index change inside the tube can certainly lead to pronounced mode shifts for transmission spectra observation as shown in Fig. 4(a). Both curves were measured with the same tube (D = 20 μm, T = 0.5 μm). The black line is the transmission spectrum measured in air (n = 1.000) and the red line is that measured with liquid IPA (n = 1.375) in a tube. Obviously, a 65.3 nm spectral shift is observed and guided by the dot-dash line arrow in Fig. 4(a) with the assistance of analytical calculation based on the Mie scattering theory.[21,48,50] This rigorous theory can give accurate resonance properties and parameters for small tubular microcavities, and is suitable for multi-layer structures like liquid-in-tube configurations (an additional short description and explanation about Mie scattering also shown in the ESI†).[21,48] Such a spectral shift corresponds to the azimuthal number m = 55. Fig. 4(b) shows the corresponding simulation curve (solid circle and red line) between the TM mode position m = 55 and the refractive index n inside the hollow structure for the measured tubular microcavity (D = 20 μm, T = 0.5 μm) in Fig. 4(a). The sensitivity (the slope of solid circle and red line in Fig. 4(b)) gradually increases along with n changes from 1.0 to 1.4. Such non-linear sensitivity can be simply regarded as the change of optical field distribution in the microcavity and its interactional evanescent tail.[29] The measured values for m = 55 in air and IPA represented by blue asterisks agree well with the simulated curve. The insets are the corresponding optical field distributions for the mode m = 55 in air and IPA from the simulation. Based on the enlarged views, the evanescent field penetrates more into surrounding media when the medium n increases, which improves the sensitivity.[21]

Based on the above discussion, a nominal sensitivity of 174 nm RIU^{-1} can be achieved from air to IPA. However, as was claimed, the sensitivity non-linearly increases when the refractive index n of the liquid inside increases. To prove this, transmission spectral measurements of the same tubular microcavity are carried out by successively filling with different liquids of slight n changes. Three liquids were utilized as described in the Optofluidic setup section. Fig. 4(c) exhibits the corresponding transmission spectra for three liquids (n = 1.370, 1.375, 1.385) inside the tube (*i.e.* liquid-in-tube configuration). Red shifts of the resonant modes are observed with increasing n. Detailed shift values are exhibited in the lower part of the figure. The maximum sensitivity reaches as high as 390 nm RIU^{-1}, which is much higher than the above value (174 nm RIU^{-1} from air to IPA). The solid lines in Fig. 4(d) are the corresponding mode position curves simulated for modes m = 55, 56, and 57, and well agree with the measured values in Fig. 4(c), which are also marked by the scattered points (inverted triangle, rhombus, and upward triangle) in Fig. 4(d).

It is noticed that the sensitivity for smaller azimuthal number WGMs is higher than that for bigger ones, as implied by the wavelength shifts (marked in Fig. 4(c)). For example, the sensitivities are 350, 371, and 390 nm RIU^{-1} for m = 57, 56, and 55, respectively, which means that the sensitivity is higher in longer wavelengths. This phenomenon can be

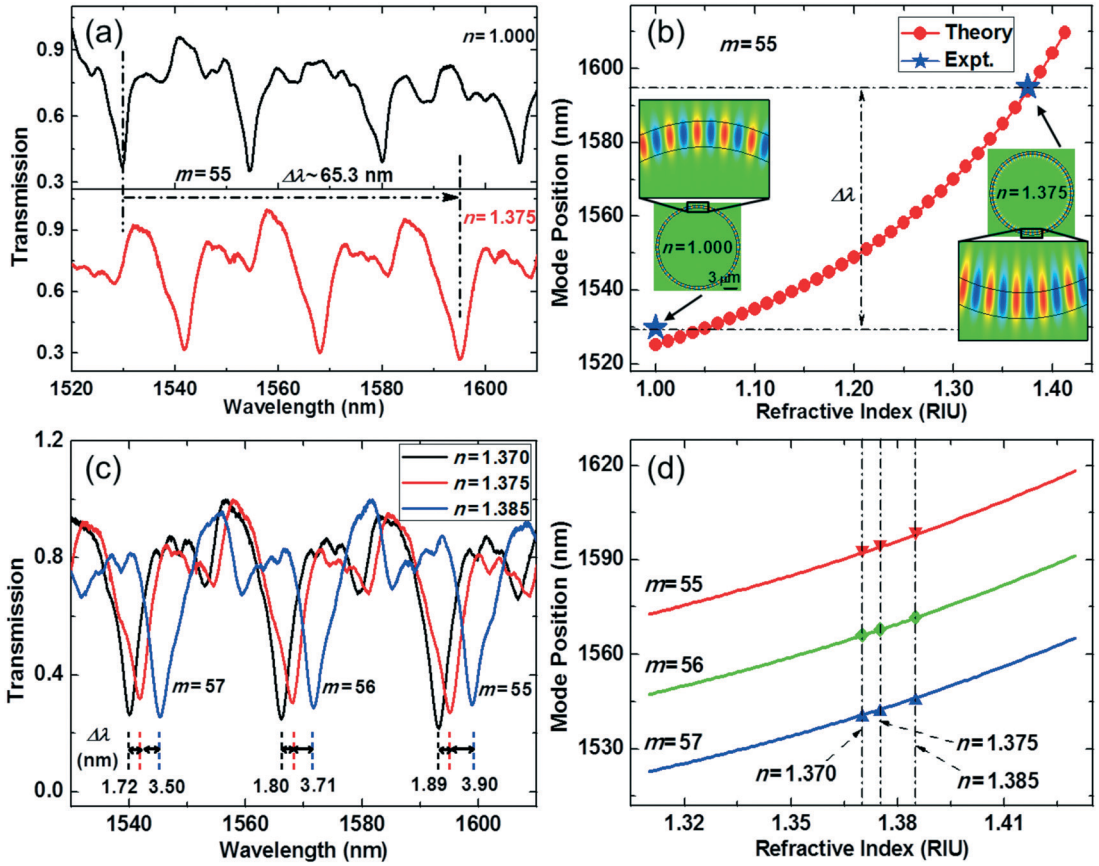

Fig. 4 Liquid sensing based on WGM mode shifts. (a) Transmission spectra of a tubular microcavity (D = 20 μm, T = 0.5 μm) filled with different media (air n = 1.000 and liquid IPA n = 1.375). The WGM shifts for mode m = 55 are about 65.3 nm. (b) Simulated mode positions as a function of filled medium with refractive index n inside a tube for m = 55 mode in (a). Blue asterisks represent the measured positions in (a). Insets are the corresponding optical field distributions and enlarged views for m = 55 with n = 1.000 and 1.375. (c) Transmission spectra of the same tube as (a) filled with liquids of various n (from 1.370 to 1.375 to 1.385). Its bottom part displays the mode shift. (d) Simulated mode positions for modes m = 55, 56 and 57 with different refractive indices inside a tube. The scattered points are experimental values taken from (c).

considered from this aspect: since the azimuthal number m represents the number of nodes dividing the whole optical field around a cavity, a larger azimuthal number means that the resonator can be divided into more nodes;[29] this can certainly enhance the optical field confinement in the microcavity itself and less light would leak out into the surrounding media, which thus reduces the sensitivity.

Besides sensitivity S, detection limit N_{DL} is another important parameter for evaluating the overall sensing ability of an optical refractometer. It can be calculated by $N_{DL} = \lambda_{RS}/S = \lambda/(50QS)$,[21] where λ_{RS} is the sensing resolution. Based on our typical experimental spectra (S = 390, Q = 2000), the calculated N_{DL} of our fabricated tubular microcavity is in the order of 10^{-5} RIU, ranging from 7×10^{-5} to 1×10^{-5} RIU, which is better than that of tubular microcavities fabricated *via* the rolled-up method,[17,29] which is in the order of 10^{-4} RIU.

Integration with coupled waveguides

Although a fiber taper is often applied for transmission spectral measurement, a fully integrated waveguide instead of a fiber taper could enable direct coupling to optical components and offer a reliable sensing device for applications. Hence, a nanophotonic coupling waveguide was placed underneath tubular microcavities to accomplish a fully integrated tubular optofluidic refractometer. As schematically shown in Fig. 5(a), a 500 nm-thick SiO_2 layer was first angle-deposited on the glass substrate by electron beam evaporation. A high deposition rate (3.0 Å s^{-1}) and a 60° glancing angle were adopted during the SiO_2 layer deposition process to obtain a relatively low n (around 1.35),[19] which was lower than the refractive index (1.48) of the resist used and guaranteed the waveguide effect in our written structure.[51–54] After deposition, a fully integrated device, composed of a tubular microcavity with liquid reservoirs and a coupled waveguide, was directly fabricated by TPP (sketched in Fig. 5(a) with a top-view optical microscopy image shown in Fig. 5(b)). Both the height and width of the waveguide are 1 μm underneath the tube. At both ends, grating couplers are designed for coupling light into and out of the waveguide with external cleaved SMF-28e optical fibers. The design of the grating is based on the grating coupling equation for the first-order diffraction: $\Lambda = \lambda/(N_{eff} - \sin\theta)$,[55] where Λ is the grating period, λ is the wavelength and θ is the coupling

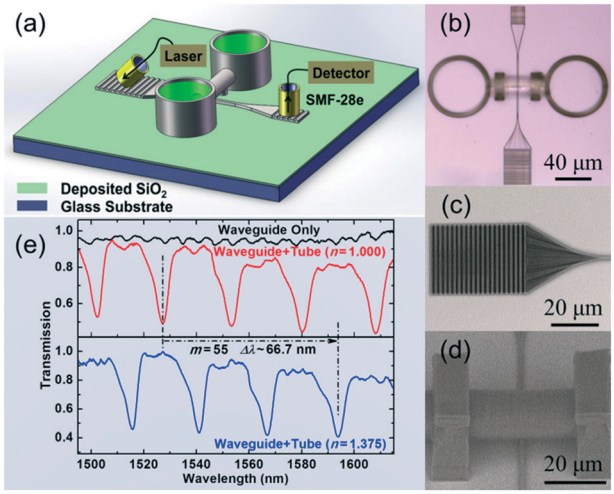

Fig. 5 Optofluidic refractometer coupled with an on-chip waveguide. (a) Sketch of a fully integrated tubular device combining a microcavity and a waveguide. The transmission characterization is based on grating couplers, fiber-in and fiber-out configurations. (b) Top-view optical microscopy image of a whole fabricated tubular device. (c) Enlarged SEM image of the grating coupler and taper transition region. (d) Enlarged side view image of the coupling region. (e) Transmission spectra of a fabricated tubular microcavity (D = 20 μm, T = 0.5 μm) filled with air n = 1.000 (red line) and liquid IPA n = 1.375 (blue). The black curve corresponds to the transmission spectrum of a stand-alone waveguide for reference.

angle from the normal direction. In this work, the grating period is set as 2 μm, with 50% duty cycle and a depth of 500 nm (Fig. 5(c)). The input light should be oblique-in, as shown in Fig. 5(a), with an incident angle of 45–55°. The back diffraction by the grating can enhance the input light beam transmitting towards the collection path and increase the signal-to-noise ratio of transmission measurement. With this side-pump configuration, the input grating port's size (30 × 40 μm^2) is also larger than that of the output port (15 × 20 μm^2). Here, the taper transition regions are designed to gradually decrease and thus accommodate the size mismatch between the grating couplers and the waveguide, which can improve the transmission efficiency. The vertical gap between the tubular microcavity and the waveguide can be well designed and set to about 300 nm, which ensures effective light coupling for transmission spectral measurement in the current experiment. An enlarged side view of a tubular microcavity integrated with a coupled waveguide is shown in Fig. 5(d), which was written in one-step formation.

The transmission spectra of a fully integrated tubular microcavity (D = 20 μm, T = 0.5 μm) are shown in Fig. 5(e) for the pure waveguide (Waveguide Only, black line) and a microtube coupled with the waveguide (Waveguide+Tube, red line for the surrounding medium n = 1.000 and blue line for n = 1.375). Obvious WGM dips can be observed in the red spectrum for the microtube coupled with the waveguide. After filling the hollow core with IPA (n = 1.375), instead of the original air (n = 1.000), a significant WGM red shift can be observed as plotted in the blue spectrum. The shift distance for the mode m = 55 is about 66.7 nm with the assistance of analytical calculation, close to the value (around 65.3 nm) in Fig. 4(a), which applied a tapered fiber as the coupled waveguide.

Table 1 shows a comparison of experimentally demonstrated schemes related to the structure designed in this work. Normally, refractometers based on pulled capillaries can be easily fabricated (only need one step),[57] but they are hardly compatible with Si technology for further on-chip integration. Rolled-up technology can also realize liquid-in-tube sensing, but the fabrication process is relatively complex, as it needs some additional steps with great care, like socket

Table 1 Summary and comparison of experimentally demonstrated "liquid-in-tube refractometers" and "microtubes integrated with waveguides". This mainly includes the device structure, material, parameter and sensitivity

Name[Ref.]	Schematic	Material system	D/T/channel cross-section (μm/μm/μm^2)	Sensitivity (nm per RIU)
Liquid ring resonator[56]		Glass capillary and fiber	212/0/3.1 × 10^4	800 (n_{liquid} ≈ 1.43)
Glass ring resonator[15]		SiO_2 nanomembrane	13/0.21/133	880 (n_{liquid} ≈ 1.34)
Thin capillary[57]		Glass capillary and fiber	80/2/5024	80.14 (n_{liquid} ≈ 1.36)
Microtube with waveguide[52]		GaAs/InGaAs microtube and Si waveguide	—	—
Microtube with waveguide[53]		TiO_2 microtube with Si waveguide	—	—
Optofluidic microtube with waveguide[This work]		Polymer (IP-L 780)	20/0.5/314	390 (n_{liquid} ≈ 1.38)

pair fabrication, tubular microcavity transfer by micro-operation, microtube re-fixing and others.[15] The preparation of rolled-up tubes integrated with waveguides is similar; it also needs cautious transfer of tubes[52] or error-prone multiple lithography.[53] Compared with the above technologies, the fabrication of integrated optofluidic microtubes with waveguides in this work using TPP is easy and flexible; what we need in this technology is to input the designed structure and press the start button. Also, by optimizing the writing parameters and speed, the whole structure can be finished within 2–3 hours, which is admirable for timely feedback and further structure optimization. Besides, the sensitivity of our fabricated tubular sensor is promising, considering its relatively thick wall thickness of 0.5 μm, and it can also be further improved with reducing the thickness.

Overall, in our flexible TPP process, we can construct unique hollow tubes, affiliated reservoirs for liquid injection, and integrated waveguides for coupling on-a-chip into a tubular optofluidic refractometer. Liquid flow inside the tubular device could be realized by injecting liquid into one reservoir while draining at the other reservoir if a microfluidic chip is adopted. By changing liquids continuously, this device can qualify real-time sensing for refractive index changes of liquids flowing inside. Furthermore, a long tubular microcavity integrated with multi-channel waveguides could enable large-scale parallel optofluidic sensing for testing a tiny sample volume.[58]

Conclusions

A direct laser writing technique based on two-photon polymerization has been successfully employed to fabricate high-Q tubular microcavities integrated with liquid reservoirs and coupled waveguides for optofluidic sensing. Such a method can offer broad tuning of the tube diameter and length. The uniformity and reliability of their optical resonance properties were optimized with writing directions for high Q-factors and mechanical stability. The Q values of the tubular devices measured can reach as high as 3600 for the microtube with a diameter of 15 μm and a wall thickness of 0.6 μm. The liquid sensing capability based on WGM shifts was demonstrated under the liquid-in-tube configuration. A maximal sensitivity of 390 nm RIU^{-1} was achieved at a working wavelength of around 1595 nm, and the detection limit can reach the order of 10^{-5} RIU. Such a highly integrative optofluidic refractometer based on tubular microcavities could offer a new design route for lab-on-a-chip systems as well as optical integrative microsystems with multifunctions.[51–54,59,60]

Acknowledgements

This work is supported by the Natural Science Foundation of China (No. 51322201 and 51302039), the Science and Technology Commission of Shanghai Municipality (No. 14JC1400200) and the Open Foundation of Key Laboratory of Nanodevices and Applications, SINANO, CAS (No. 15ZS07). Part of the experimental work is carried out at Fudan Nanofabrication Laboratory.

References

1 X. D. Fan, I. M. White, S. I. Shopova, H. Y. Zhu, J. D. Suter and Y. Sun, *Anal. Chim. Acta*, 2008, **620**, 8–26.
2 K. J. Vahala, *Nature*, 2003, **424**, 839–846.
3 F. Vollmer and S. Arnold, *Nat. Methods*, 2008, **5**, 591–596.
4 J. Homola, S. S. Yee and G. Gauglitz, *Sens. Actuators, B*, 1999, **54**, 3–15.
5 D. Psaltis, S. R. Quake and C. Yang, *Nature*, 2006, **442**, 381–386.
6 C. Monat, P. Domachuk and B. J. Eggleton, *Nat. Photonics*, 2007, **1**, 106–114.
7 J. Homola, *Sens. Actuators, B*, 1997, **41**, 207–211.
8 K. A. Willets and R. P. V. Duyne, *Annu. Rev. Phys. Chem.*, 2007, **58**, 267–297.
9 V. S. Y. Lin, K. Motesharei, K. S. Dancil, M. J. Sailor and M. R. Ghadiri, *Science*, 1997, **278**, 840–843.
10 P. Kozma, F. Kehl, E. Ehrentreich-Förster, C. Stamm and F. F. Bier, *Biosens. Bioelectron.*, 2014, **58**, 287–307.
11 N. Skivesen, R. Horvath and H. C. Pedersen, *Opt. Lett.*, 2005, **30**, 1659–1661.
12 Y. F. Mei, G. S. Huang, A. A. Solovev, E. B. Ureña, I. Monch, F. Ding, T. Reindl, R. K. Y. Fu, P. K. Chu and O. G. Schmidt, *Adv. Mater.*, 2008, **20**, 4085–4090.
13 J. G. Zhu, S. K. Ozdemir, Y. F. Xiao, L. Lin, L. He, D. R. Chen and L. Yang, *Nat. Photonics*, 2009, **4**, 46–49.
14 M. Li, X. Wu, L. Y. Liu, X. D. Fan and L. Xu, *Anal. Chem.*, 2013, **85**, 9328–9332.
15 E. J. Smith, W. Xi, D. Makarov, I. Monch, S. Harazim, V. A. Bolanos Quinones, C. K. Schmidt, Y. F. Mei, S. Sanchez and O. G. Schmidt, *Lab Chip*, 2012, **12**, 1917.
16 X. D. Fan and S. H. Yun, *Nat. Methods*, 2014, **11**, 141–147.
17 S. M. Harazim, V. A. Bolaños Quiñones, S. Kiravittaya, S. Sanchez and O. G. Schmidt, *Lab Chip*, 2012, **12**, 2649–2655.
18 H. Chandrahalim, Q. S. Chen, A. A. Said, M. Dugan and X. D. Fan, *Lab Chip*, 2015, **15**, 2335–2340.
19 J. Wang, T. R. Zhan, G. S. Huang, P. K. Chu and Y. F. Mei, *Laser Photonics Rev.*, 2014, **8**, 521.
20 D. K. Armani, T. J. Kippenberg, S. M. Spillane and K. J. Vahala, *Nature*, 2003, **421**, 925–928.
21 F. Y. Zhao, T. R. Zhan, G. S. Huang, Y. F. Mei and X. H. Hu, *Lab Chip*, 2012, **12**, 3798–3802.
22 Y. Z. Yan, C. L. Zou, S. B. Yan, F. W. Sun, Z. Ji, J. Liu, Y. G. Zhang, L. Wang, C. Y. Xue, W. D. Zhang, Z. F. Han and J. J. Xiong, *Opt. Express*, 2011, **19**, 5753–5759.
23 H. Zhu, I. M. White, J. D. Suter, P. S. Dale and X. Fan, *Opt. Express*, 2007, **15**, 9139–9146.
24 J. Zhang, J. Zhong, Y. F. Fang, J. Wang, G. S. Huang, X. G. Cui and Y. F. Mei, *Nanoscale*, 2014, **6**, 13646–13650.
25 J. Trommer, S. Bottner, S. Li, S. Kiravittaya, M. R. Jorgensen and O. G. Schmidt, *Opt. Lett.*, 2014, **39**, 6335–6338.
26 S. Li, L. Ma, S. Böttner, Y. Mei, M. R. Jorgensen, S. Kiravittaya and O. G. Schmidt, *Phys. Rev. A*, 2013, **88**, 033833.

27 J. Ward and O. Benson, *Laser Photonics Rev.*, 2011, **5**, 553–570.
28 W. Fang, D. B. Buchholz, R. C. Bailey, J. T. Hupp, R. P. H. Chang and H. Cao, *Appl. Phys. Lett.*, 2004, **85**, 3666–3668.
29 G. S. Huang, V. A. Bolaños Quiñones, F. Ding, S. Kiravittaya, Y. F. Mei and O. G. Schmidt, *ACS Nano*, 2010, **4**, 3123–3130.
30 S. W. Tang, Y. F. Fang, Z. W. Liu, L. Zhou and Y. F. Mei, *Lab Chip*, 2016, **16**, 182–187.
31 O. G. Schmidt and K. Eberl, *Nature*, 2001, **410**, 168.
32 C. M. B. Ho, S. H. Ng, K. H. H. Li and Y.-J. Yoon, *Lab Chip*, 2015, **15**, 3627.
33 J. Wang, H. Xia, B. B. Xu, L. G. Niu, D. Wu, Q. D. Chen and H. B. Sun, *Opt. Lett.*, 2009, **34**, 581–583.
34 B. H. Cumpston, S. P. Ananthavel, S. Barlow, D. L. Dyer, J. E. Ehrlich, L. L. Erskine, A. A. Heikal, S. M. Kuebler, I. Y. S. Lee, D. M. Maughon, J. Q. Qin, H. RoÈckel, M. Rumi, X. L. Wu, S. R. Marder and J. W. Perry, *Nature*, 1999, **398**, 51–54.
35 J. K. Gansel, M. Thiel, M. S. Rill, M. Decker, K. Bade, V. Saile, G. V. Freymann, S. Linden and M. Wegener, *Science*, 2009, **325**, 1513–1515.
36 L. J. Li, E. Gershgoren, G. Kumi, W. Y. Chen, P. T. Ho, W. N. Herman and J. T. Fourkas, *Adv. Mater.*, 2008, **20**, 3668–3671.
37 Z. P. Liu, Y. Li, Y. F. Xiao, B. B. Li, X. F. Jiang, Y. Qin, X. B. Feng, H. Yang and Q. H. Gong, *Appl. Phys. Lett.*, 2010, **97**, 211105.
38 A. W. Schell, J. Kaschke, J. Fischer, R. Henze, J. Wolters, M. Wegener and O. Benson, *Sci. Rep.*, 2013, **3**, 1577.
39 T. Grossmann, S. Schleede, M. Hauser, T. Beck, M. Thiel, G. V. Freymann, T. Mappes and H. Kalt, *Opt. Express*, 2011, **19**, 11451–11456.
40 M. Schumann, T. Buckmann, N. Gruhler, M. Wegener and W. Pernice, *Light: Sci. Appl.*, 2014, **3**, e175.
41 J. T. Lin, S. J. Yu, Y. G. Ma, W. Fang, F. He, L. L. Qiao, L. M. Tong, Y. Cheng and Z. Z. Xu, *Opt. Express*, 2012, **20**, 10212–10217.
42 T. Carmon, L. Yang and K. J. Vahala, *Opt. Express*, 2004, **12**, 4742–4750.
43 H. Chen, L. Kong and Y. Wang, *J. Membr. Sci.*, 2015, **487**, 109–116.
44 J. Wang, G. S. Huang and Y. F. Mei, *Chem. Vap. Depositon*, 2014, **20**, 103–111.
45 M. L. Gorodetsky and V. S. Ilchenko, *J. Opt. Soc. Am. B*, 1999, **16**, 147–154.
46 B. E. Little, *J. Lightwave Technol.*, 1999, **17**, 704–715.
47 T. J. Kippenberg, S. M. Spillane and K. J. Vahala, *Phys. Rev. Lett.*, 2004, **93**, 083904.
48 J. Wang, T. Zhan, G. S. Huang, X. Cui, X. Hu and Y. F. Mei, *Opt. Express*, 2012, **20**, 18555.
49 M. Cai, O. Painter and K. J. Vahala, *Phys. Rev. Lett.*, 2000, **85**, 74–77.
50 C. C. Lam, P. T. Leung and K. Young, *J. Opt. Soc. Am. B*, 1992, **9**, 1585–1592.
51 Z. Tian, V. Veerasubramanian, P. Bianucci, S. Mukherjee, Z. Mi, A. G. Kirk and D. V. Plant, *Opt. Express*, 2011, **19**, 12164–12171.
52 Q. Zhong, Z. Tian, V. Veerasubramanian, M. H. T. Dastjerdi, Z. Mi and D. V. Plant, *Opt. Lett.*, 2014, **39**, 2699–2702.
53 A. Madani, M. Kleinert, D. Stolarek, L. Zimmermann, L. Ma and O. G. Schmidt, *Opt. Lett.*, 2015, **40**, 3826–3829.
54 X. Yu, E. Arbabi, L. L. Goddard, X. Li and X. Chen, *Appl. Phys. Lett.*, 2015, **107**, 031102.
55 S. Koseki, *PhD Thesis*, Stanford University, 2008, p. 9.
56 M. Sumetsky, R. S. Windeler, Y. Dulashko and X. Fan, *Opt. Express*, 2007, **15**, 14376.
57 Y. Luo, X. Chen, M. Xu, Z. Chen and X. Fan, *Opt. Laser Technol.*, 2014, **56**, 12–14.
58 I. M. White, H. Zhu, J. D. Suter, N. M. Hanumegowda, H. Overys, M. Zourob and X. Fan, *IEEE Sens. J.*, 2007, **7**, 28–35.
59 H. Rokhsari and K. J. Vahala, *Phys. Rev. Lett.*, 2004, **92**, 253905.
60 S. Böttner, S. L. Li, M. R. Jorgensen and O. G. Schmidt, *Appl. Phys. Lett.*, 2013, **102**, 251119.

